ELSEVIER

Contents lists available at ScienceDirect

Extreme Mechanics Letters

journal homepage: www.elsevier.com/locate/eml



Effect of tension/compression asymmetry and anisotropy on the response of pseudoelastic NiTi tubes under equibiaxial stress



Karlos Kazinakis, Stelios Kyriakides*, Chad M. Landis

Research Center for Mechanics of Solids, Structures & Materials, ASE, The University of Texas at Austin, Austin, TX 78712, USA

ARTICLE INFO

Article history:
Received 10 December 2021
Received in revised form 17 February 2022
Accepted 7 March 2022
Available online 16 March 2022

Keywords:
Equibiaxial stress
NiTi tubes
Pseudoelasticity
Tension/compression asymmetry
Anisotropy
Inhomogeneous deformation
Analysis

ABSTRACT

The stress-strain response and inhomogeneous deformation of pseudoelastic NiTi tubes loaded under combined axial force and internal pressure are governed not only by the well-known tension/compression asymmetry but also anisotropy (Bechle and Kyriakides, 2016). This behavior was simulated successfully in Kazinakis et al. (2022) using a finite element analysis coupled to a recently developed constitutive model that incorporates these key material characteristics. Interestingly, equibiaxial tension induces monotonic stress-strain hystereses and nearly homogeneous deformations, but with the hoop transformation strain being approximately double the axial one. This letter uses analysis to highlight how the tension/compression asymmetry and anisotropy individually influence the predictions of this experiment. When both asymmetry and anisotropy are included, the analysis captures the level of transformations stresses and the extent of axial strain, overpredicting the hoop strain by a small amount. The hardening is somewhat reduced compared to the experiment allowing weak and diffuse inhomogeneous deformation to develop. In the absence of anisotropy, the hoop and axial hystereses coincide with much higher stresses, and strains that lie between the experimental values, while the tube deforms uniformly. If the model is assumed symmetric with the properties of the hardening uniaxial compression, the behavior is the same as that of the previous case. When the model is calibrated instead to the partially unstable uniaxial tensile response, the analysis predicts again coincident stress-average strain hystereses with lower stress plateaus than measured and strongly inhomogeneous deformation.

© 2022 Elsevier Ltd. All rights reserved.

1. Introduction

The unique property of nearly equiatomic NiTi to fully recover from strains of several percent is associated with solidstate transformations between the austenitic (A) and martensitic (M) phases. It is well established that the material exhibits tension/compression asymmetry as illustrated for example in Fig. 1a, which compares the uniaxial tensile and compressive nominal stress-elongation/shortening responses of NiTi tubes at room temperature (from [1]; see also [2-4] among others). Both responses are pseudoelastic in that the transformation induced strain is recoverable. Under axial tension, transformation starts at about 460 MPa and leads to localized deformation in the form of helical bands of about 7% strain (Fig. 1b) with the stress remaining nearly constant. On unloading, the material reverts back to austenite at a stress of about 235 MPa and is associated with multi-pronged bands. By contrast under compression, transformation initiates at a stress of about 630 MPa, and the response monotonically increases until it is completed at about

4.1%. Furthermore, the deformation is essentially homogeneous (Fig. 1c).

Biaxial loadings of combined axial-torsion (e.g., [6-8]) and axial-internal pressure loads [5] on tubes revealed more complex manifestations of the tension/compression asymmetry. For example, Fig. 2a shows the stress-average strain responses in the axial $(\sigma_x - \overline{\varepsilon}_x)$ and hoop $(\sigma_\theta - \overline{\varepsilon}_\theta)$ direction recorded under equibiaxial tension $(\sigma_x = \sigma_\theta)$. Both are monotonic closed hystereses, but whereas the hoop response extends to a strain of 2.86% the axial one ends at 1.56%. This is a form of anisotropy presumably introduced by the manufacturing process. The corresponding deformed images of the test section in Fig. 2b show the axial strain to evolve homogeneously and the hoop strain to exhibit very mild inhomogeneity with axially oriented patterns. Experiments were conducted for biaxiality ratios, $\sigma_x = \alpha \sigma_\theta$, ranging from $\alpha = -1$ to uniaxial tension ($\alpha = \infty$). The monotonic behavior and nearly homogeneous deformation were observed only for a narrow range of biaxiality ratios, α , in the neighborhood of the equibiaxial tension. For higher and lower stress ratios deformation localized akin to the behavior of uniaxial tension in Fig. 1b (see [5]).

The pattern-rich behaviors observed in the internal axial forceinternal pressure biaxial experiments were simulated successfully

^{*} Corresponding author. E-mail address: skk@mail.utexas.edu (S. Kyriakides).

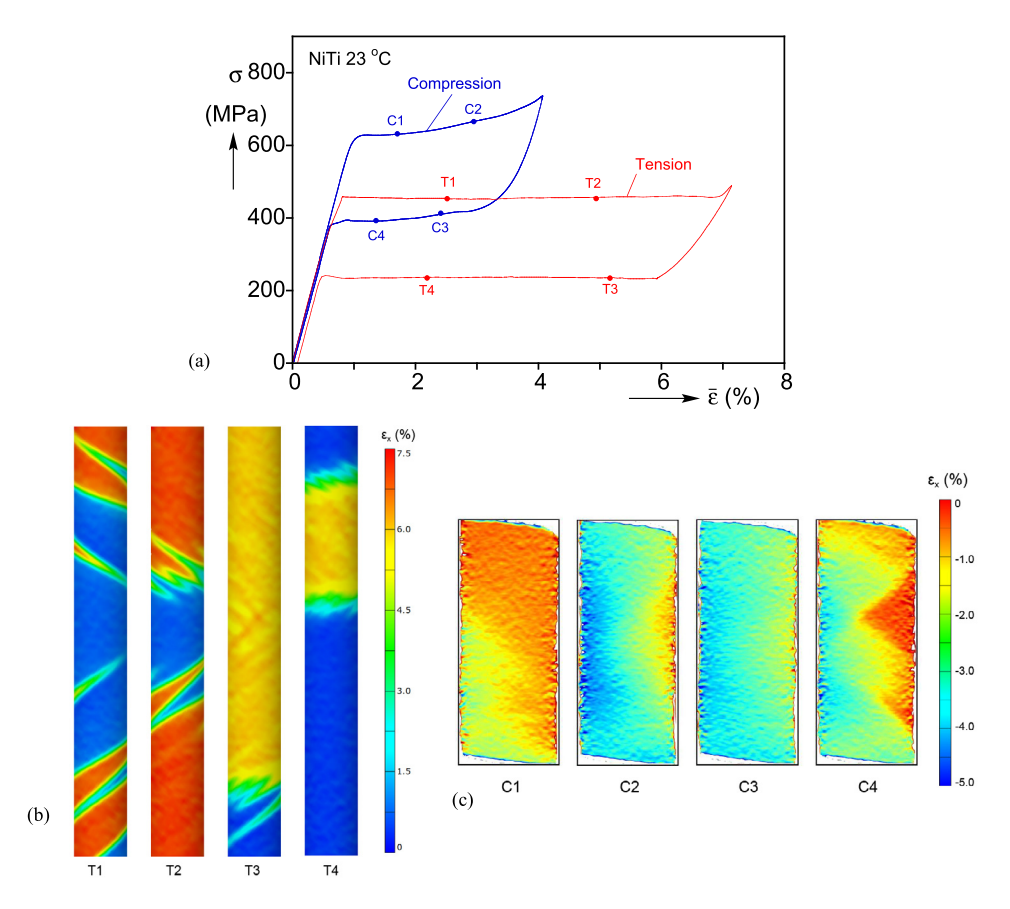


Fig. 1. (a) Tensile and compressive axial stress-elongation/shortening responses exhibiting asymmetry. Select DIC deformation contours corresponding to bullets on (b) the tensile response, and (c) the compressive response [1].

in [9] using a finite element model coupled to a phenomenological constitutive model. The model incorporates the tension-compression asymmetry including the associated softening and hardening behaviors previously developed by our group [10–13], and is extended to include the anisotropy observed under biaxial stress states. The present letter concentrates on the equibiaxial loading case, $\sigma_x = \sigma_\theta$, and uses analysis to highlight the important effects of tension/compression asymmetry and anisotropy individually and jointly on the calculated response and deformation patterns.

2. Analysis

a. Finite Element Model

A tube of length L, diameter D, and wall thickness t, $\{50 \times 6.33 \times 0.273\}$ mm, is meshed using second-order reduced integration solid elements (ABAQUS C3D20R) with one element through the thickness, 120 around the circumference and 314 along the length (Fig. 3). The model is pressurized internally under volume control using a cavity formed by incompressible fluid elements F3D4 in the body and F3D3 at the ends caps. The ends at x=0 and L are free to expand radially while the average in-plane nodal displacements and rotations at the ends are prescribed to be zero (i.e., $\sum_{i}^{n} u_{yi} = \sum_{i}^{n} u_{zi} = \sum_{i}^{n} u_{\theta i} = 0$). The axial displacement of all nodes at x=0 is made zero while at x=L it is assigned a stress σ_x .

The two stresses are related to the axial force, *F*, and internal pressure, *P*, through

$$\sigma_{x} = \frac{F}{2\pi Rt} + \frac{PR}{2t}$$
 and $\sigma_{\theta} = \frac{PR}{t}$. (1)

Equibiaxial loading, $\sigma_x = \sigma_\theta$, is achieved using a control loop in a UAMP as follows. The change in volume of the fluid inside the cavity is prescribed incrementally, the resultant pressure is measured and used to calculate the required axial force increment to make the hoop and axial stresses equal. A small thickness depression is placed close to the axially free end to help trigger potential localization of deformation. The depression extends over an area of about $2t \times t/2$, is 0.02t deep, and has transition zones of t/2 all around.

b. Constitutive Model

A more compact version of the constitutive model presented in [9] is included here in order to familiarize the reader with the different versions of it used in the analyses that follow. The strain increment is decomposed into elastic and transformation components,

$$\dot{\varepsilon}_{ij} = \dot{\varepsilon}_{ij}^{\ell} + \dot{\varepsilon}_{ij}^{t}. \tag{2}$$

The elastic deformation is isotropic and related to the stress increment by

$$\dot{\sigma}_{ij} = C_{ijkl}(\dot{\varepsilon}_{kl} - \dot{\varepsilon}_{kl}^t),\tag{3}$$

and is enclosed by a transformation surface that obeys kinematic hardening defined by

$$\Phi = \frac{3}{2} (s_{ij} - s_{ij}^B)(s_{ij} - s_{ij}^B) - \sigma_o^2 = 0; \tag{4}$$

where s_{ij} and s_{ij}^B are the deviatoric components of stress and back stress, and σ_o represents the size of the transformation surface. The transformation strain follows an associated flow rule and the

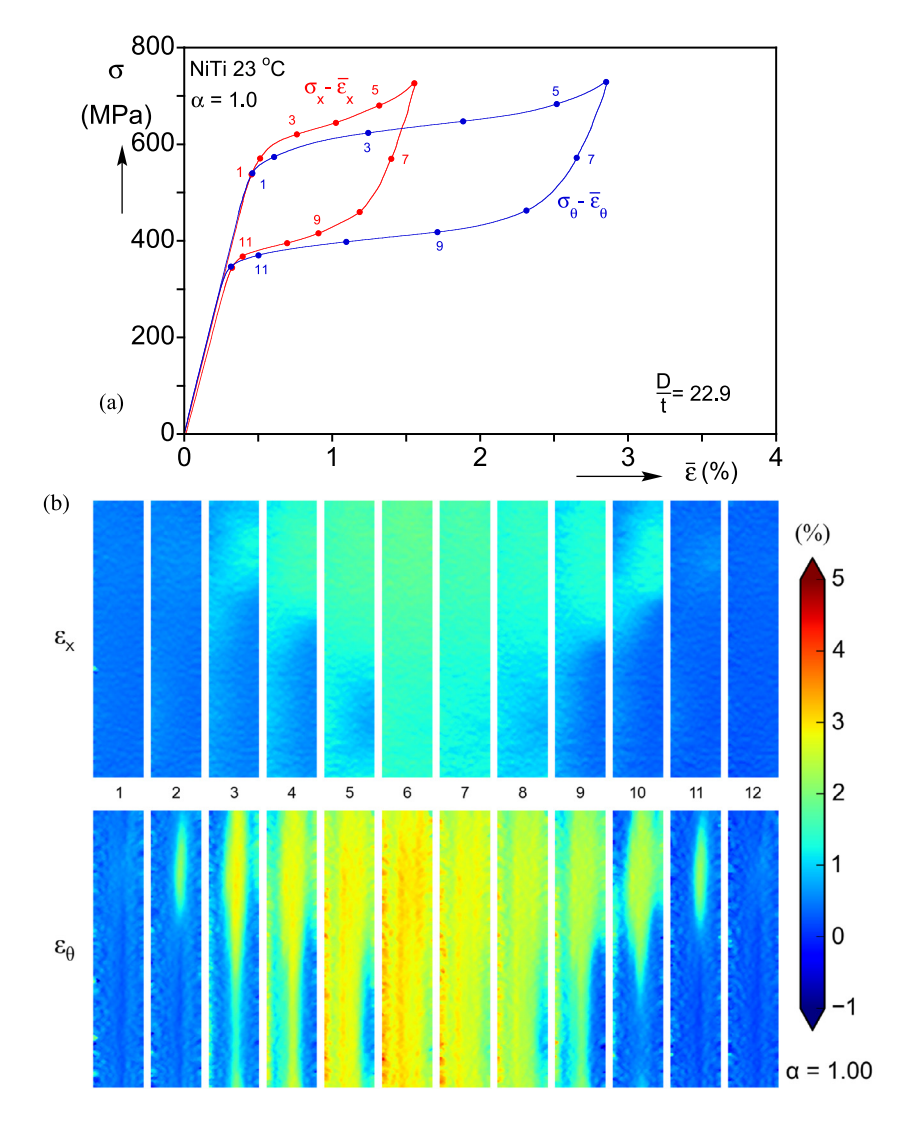


Fig. 2. (a) Axial and hoop stress-average strain responses recorded in an equibiaxial experiment on pseudoelastic NiTi, and (b) corresponding sequences of full-field DIC strain contours [5].

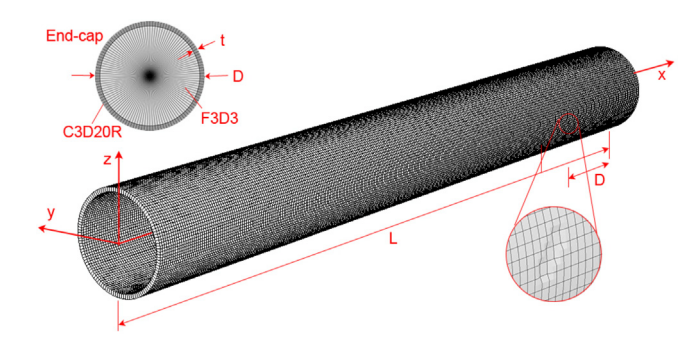


Fig. 3. The geometry and finite element mesh of the model tube used in the analysis.

back stress is derived from a potential as follows

$$\sigma_{ij}^{B} = \frac{\partial \psi^{t}}{\partial \varepsilon_{ii}^{t}}.$$
 (5)

The tension/compression asymmetry is introduced through the following representation of this potential

$$\psi^t = \xi \psi_c^t(\varepsilon_e^t) + (1 - \xi)\psi_t^t(\varepsilon_e^t), \tag{6}$$

where ψ^t_c and ψ^t_t are calibrated to the measured uniaxial compression and tension stress–transformation strain responses; ε^t_e is an "equivalent" transformation strain and $\xi \in [0,1]$ a weight function. Jiang et al. [10] adopted the following definition of the equivalent strain

$$\varepsilon_e^t = J_2' f(J_r'), \quad J_r' = J_3' / J_2',$$
 (7)

where $f(J'_r)$ is a scale function and J'_i are the invariants of the deviatoric transformation strain, e^t .

Kazinakis et al. [9] introduced anisotropy to the model by two affine mappings of the transformation strains

$$\tilde{\mathbf{e}}^t = \mathbf{D}_1 \mathbf{e}^t, \quad \hat{\mathbf{e}}^t = \mathbf{D}_2 \mathbf{e}^t. \tag{8}$$

The modified invariants and equivalent strain then become:

$$\tilde{J}_{2}' = (2\tilde{e}_{ij}^{t}\tilde{e}_{ij}^{t}/3)^{1/2}, \hat{J}'_{3} = (4\tilde{e}_{ij}^{t}\tilde{e}_{jk}^{t}\tilde{e}_{ki}^{t}/3)^{1/3}, \text{ and}
\tilde{\varepsilon}_{e}^{t} = \tilde{J}_{2}'f(\tilde{J}'_{r}), \quad \tilde{J}'_{r} = \hat{J}'_{3}/J'_{r}.$$
(9)

The scale function f is chosen as follows:

$$f\left(\tilde{J'}_r\right) = \cos\{\cos^{-1}[1 - a(\tilde{J'}_r^3 + 1)]/c\},$$
 (10)

with parameters a=0.736 and c=2.026. Here $\tilde{J}'_r=1$ represents uniaxial extension (f=1) and $\tilde{J}'_r=-1$ uniaxial contraction (f=1)

0.525). The weight function ξ is also selected to be a function of I_r as follows:

$$\xi = \frac{f(\tilde{J}_r') - f(1)}{f(-1) - f(1)},\tag{11}$$

which facilitates the generalization of (6) to multiaxial states.

The form of the mappings \mathbf{D}_i expressed in Voigt notation is as follows:

$$\mathbf{D}_{i} = \begin{bmatrix} \mathbf{A}_{i} & \mathbf{0} \\ \mathbf{0} & \mathbf{I} \end{bmatrix}, \text{ where } \mathbf{A}_{i} = \begin{bmatrix} 1 & 0 & 0 \\ 0 & A_{i} & 1 - A_{i} \\ 0 & 1 - A_{i} & A_{i} \end{bmatrix}, i = 1, 2.$$

$$(12)$$

This single parameter mapping ensures that e_{11}^t remains unchanged, imposes transverse anisotropy and incompressibility to the transformation strains, while the shear strains remain unchanged. For added flexibility, the two invariants are mapped with different parameters: A_1 for \tilde{J}'_2 and A_2 for \tilde{J}'_3 (see Appendix B of Kazinakis et al. [9]). The back stress (5) is then written as:

$$\sigma_{ij}^{B} = \xi \frac{d\psi_{c}^{t}}{d\tilde{\varepsilon}_{e}^{t}} \frac{\partial \tilde{\varepsilon}_{e}^{t}}{\partial \varepsilon_{ij}^{t}} + (1 - \xi) \frac{d\psi_{t}^{t}}{d\tilde{\varepsilon}_{e}^{t}} \frac{\partial \tilde{\varepsilon}_{e}^{t}}{\partial \varepsilon_{ij}^{t}} + \xi'(\psi_{c}^{t} - \psi_{t}^{t}) \frac{\partial \tilde{J}_{r}'}{\partial \varepsilon_{ij}^{t}}, \text{ where}$$

$$\xi' \equiv \frac{\partial \xi}{\partial \tilde{J}_{r}'}. \tag{13}$$

Reduction to uniaxial stresses in the axial direction results in:

$$\sigma_{11t} - f(1) \frac{d\psi_t^t}{d\tilde{\varepsilon}_e^t} = \sigma_o \text{ and } |\sigma_{11c}| - f(-1) \frac{d\psi_c^t}{d\tilde{\varepsilon}_e^t} = \sigma_o.$$
 (14)

The uniaxial back stresses in the other two directions are influenced by scaling and anisotropy and they become

$$\sigma_{22t}^{B} = \sigma_{33t}^{B} = \left[\xi(\beta) \frac{d\psi_{c}^{t}}{d\tilde{\varepsilon}_{e}^{t}} + (1 - \xi(\beta)) \frac{d\psi_{t}^{t}}{d\tilde{\varepsilon}_{e}^{t}} \right] \gamma f(\beta), \tag{15a}$$

$$\left|\sigma_{22c}^{B}\right| = \left|\sigma_{33c}^{B}\right| = \left[\xi(-\beta)\frac{d\psi_{c}^{t}}{d\tilde{\varepsilon}_{e}^{t}} + (1 - \xi(-\beta))\frac{d\psi_{t}^{t}}{d\tilde{\varepsilon}_{e}^{t}}\right]\gamma f(-\beta),\tag{15b}$$

where $\beta=[(9A_2^2-9A_2+2)/2]^{1/3}$ and $\gamma=(3A_1^2-3A_1+1)^{1/2}$. The back stress potentials ψ_c^t and ψ_t^t are each calibrated to the compressive and tensile stress-average strain responses of the material as outlined in Appendix A. Fig. 4a compares the measured and fitted responses in the axial direction. The compressive fit replicates the monotonic character of the response measured in the experiment. The tensile fit exhibits softening branches that span the upper and lower stress plateau of the measured response of localization (see [14]).

The values of the anisotropy parameters $\{\beta, \gamma\} = \{0.8909,$ 0.8266} were found to produce a reasonable compromise between the measured levels of the transformation stresses and the extents of the transformation strains for a range of biaxiality stress states (see Appendix B of Kazinakis et al. [9]). The effect of the introduced anisotropy is prominently displayed in the uniaxial response in the hoop direction (Fig. 4b). The measured tensile response exhibited localized deformation patterns similar to those in the axial direction but with the extent of the transformation strain reduced. Accordingly, the up-down-up fit extends to a smaller strain than in the axial case, but still overestimates the experimental value to some degree. The corresponding compressive response is monotonic but with reduced hardening slopes, occurs at lower stress levels, and extends to larger strain than the corresponding axial response.

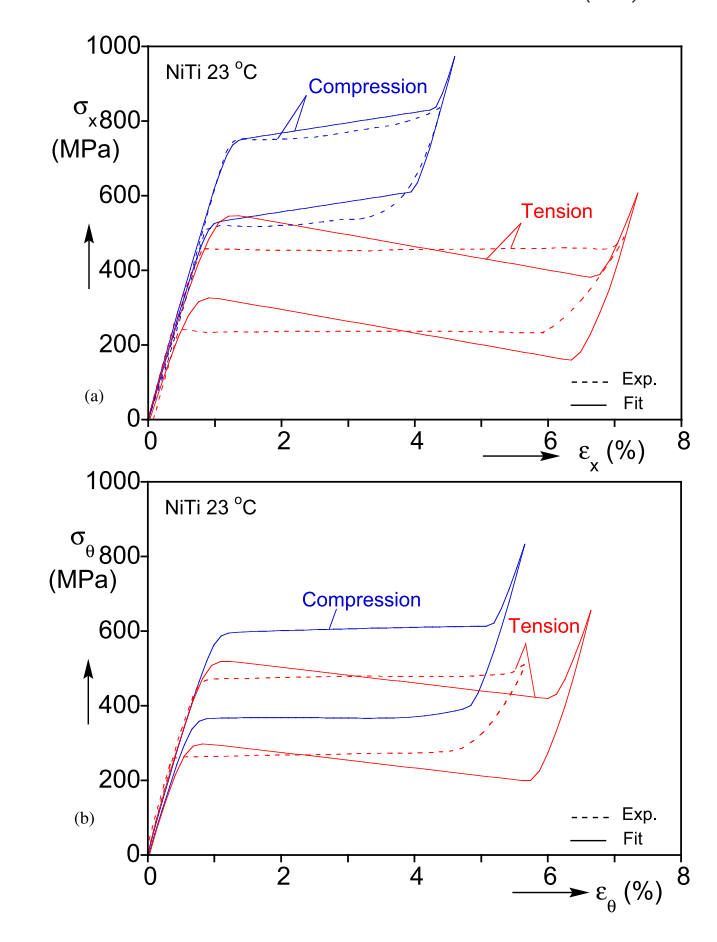


Fig. 4. (a) The axial direction tensile and compressive responses used in the analysis (solid lines) and the corresponding measured ones (dashed lines). The compressive is monotonic while the tensile one exhibits softening branches that span the experimental stress plateaus. (b) The hoop direction tensile and compressive responses adopted.

3. Analysis of the equibiaxial stress case

Kazinakis et al. [9] used the analysis outlined above to simulate the whole set of biaxial experiments reported in [5]. The calculated responses and deformation patterns were compared to the experimental results and the overall performance of the analysis was found to be reasonably good. The anisotropy adopted enabled good reproduction of the stress levels of the hysteretic responses. For axially dominant stress paths ($\alpha > 1.2$), the strain extents of the predicted responses were close to the measured values and the induced helical localization patterns compared well to those of the experiments. For hoop stress dominant paths (α < 0.85), the deformation patterns were also captured well but the strain extents of the stress plateaus were over-predicted by different degrees. This deviation is associated with the overprediction of the transformation strain observed in the pure hoop stress case in Fig. 4b, which was used in the calibration process.

Case I: Tension/Compression Asymmetry and Anisotropy

The results of the simulation for the equibiaxial case using all features of the constitutive model, summarized in the first rows of Tables 1a and 1b, are shown in Fig. 5. Fig. 5a plots the axial and hoop stress-average strain responses together with the corresponding experimental ones, and Fig. 5b presents ten deformed configurations of the model tube with the axial and hoop strains superimposed separately. The two responses are monotonic with smooth transitions at the nucleation of transformation. The transformation stress of about 625 MPa is close to

Table 1aModel parameters for different transformation features.

Model	Anisotropy \mathbf{D}_i	Scale Funct. f	Weight Funct. ξ	Back stress σ^B_{ij}	Equiv. Strain ε_e^t
Asym. + Aniso.	$\mathbf{D}_i = \begin{bmatrix} \mathbf{A}_i & 0 \\ 0 & \mathbf{I} \end{bmatrix}$	$f \in [f(1), f(-1)]$	$\xi(\tilde{J}'_r) = \frac{f(\tilde{J}'_r) - f(1)}{f(-1) - f(1)}$	$\sigma_{ij}^{B} = \xi \frac{d\psi_{c}^{t}}{d\tilde{\varepsilon}_{e}^{t}} \frac{\partial \tilde{\varepsilon}_{e}^{t}}{\partial \varepsilon_{ij}^{t}} + (1 - \xi) \frac{d\psi_{c}^{t}}{d\tilde{\varepsilon}_{e}^{t}} \frac{\partial \tilde{\varepsilon}_{e}^{t}}{\partial \varepsilon_{ij}^{t}} + (\psi_{c}^{t} - \psi_{c}^{t}) \frac{\partial \xi}{\partial \tilde{J}_{r}^{r}} \frac{\partial \tilde{J}_{r}^{r}}{\partial \varepsilon_{ij}^{t}}$	$\tilde{\varepsilon}_e^t = \tilde{J'}_2 f(\tilde{J'}_r)$
Asym.	$\mathbf{D}_i = \begin{bmatrix} \mathbf{I} & 0 \\ 0 & \mathbf{I} \end{bmatrix}$	$f \in [f(1), f(-1)]$	$\xi(J_r') = \frac{f(J_r') - f(1)}{f(-1) - f(1)}$	$\sigma_{ij}^{B} = \xi \frac{d\psi_{c}^{t}}{d\varepsilon_{e}^{t}} \frac{\partial \varepsilon_{e}^{t}}{\partial \varepsilon_{ij}^{t}} + (1 - \xi) \frac{d\psi_{t}^{t}}{d\varepsilon_{e}^{t}} \frac{\partial \varepsilon_{e}^{t}}{\partial \varepsilon_{ij}^{t}} + (\psi_{c}^{t} - \psi_{t}^{t}) \frac{\partial \xi}{\partial J_{r}^{r}} \frac{\partial J_{r}^{r}}{\partial \varepsilon_{ij}^{t}}$	$\varepsilon_e^t = J_2' f(J_r')$
Sym. C	$\mathbf{D}_i = \begin{bmatrix} \mathbf{I} & 0 \\ 0 & \mathbf{I} \end{bmatrix}$	$f = f(-1) \equiv 1$	$\dot{\xi}=1$	$\sigma^{\scriptscriptstyle B}_{ij} = rac{d\psi^t_c}{darepsilon^t_e} rac{\partial arepsilon^t_e}{\partial arepsilon^t_{ij}}$	$\varepsilon_e^t = J_2' f(-1)$
Sym. T	$\mathbf{D}_i = \begin{bmatrix} \mathbf{I} & 0 \\ 0 & \mathbf{I} \end{bmatrix}$	f = f(1) = 0.525	$\xi = 0$	$\sigma^{\scriptscriptstyle B}_{ij} = rac{d\psi^t_t}{darepsilon^c_e} rac{\partial arepsilon^t_e}{\partial arepsilon^t_i} rac{\partial arepsilon^t_e}{\partial arepsilon^t_{ij}}$	$\varepsilon_e^t = J_2' f(1)$

Table 1bModel parameters for different transformation features for equibiaxial stress

Model	Anisotropy $\{\beta, \gamma\}$	Scale Funct. f	Weight Funct. ξ	Back stress σ^B_{ij}	Equiv. Strain $arepsilon_e^t$
Asym. + Aniso.	{0.891,0.827}	$f = f(-\beta) < f(-1)$	$\xi = \xi(-\beta) < 1$	$\sigma_{x}^{B} = \sigma_{\theta}^{B} = \left(\xi(-\beta)\frac{d\psi_{c}^{t}}{d\tilde{\varepsilon}_{e}^{t}} + (1 - \xi(-\beta))\frac{d\psi_{t}^{t}}{d\tilde{\varepsilon}_{e}^{t}}\right)\gamma f(-\beta)$	$\tilde{\varepsilon}_e^t = 2\gamma \varepsilon_o^t f(-\beta)$
Asym.	{1,1}	$f = f(-1) \equiv 1$	$\xi = 1$	$\sigma_{x}^{B} = \sigma_{\theta}^{B} = f(-1) \frac{d\psi_{c}^{t}}{d\tilde{\varepsilon}_{e}^{t}}$	$\varepsilon_e^t = 2\varepsilon_o^t f(-1)$
Sym. C	{1,1}	$f = f(-1) \equiv 1$	$\xi = 1$	$\sigma_{x}^{B} = \sigma_{0}^{B} = f(-1)\frac{d\psi_{c}^{t}}{d\varepsilon_{c}^{t}}$	$\varepsilon_e^t = 2\varepsilon_o^t f(-1)$
Sym. T	{1,1}	f = f(1) = 0.525	$\xi = 0$	$\sigma_{\rm x}^{\rm B} = \sigma_{ heta}^{\rm B} = f(1) rac{d\psi_{t}^{ m t}}{darepsilon_{e}^{ m t}}$	$\varepsilon_e^t = 2\varepsilon_o^t f(1)$

the experimental value. By the completion of transformation, the stresses increase to about 660 MPa, a smaller increase than in the experiment, which exhibited higher hardening. As a consequence of the anisotropy adopted, the equibiaxial stresses are mainly influenced by the compressive potential (see first row of Table 1b; $\xi = 0.885$). Although the influence of the tensile potential is smaller, it has the effect of lowering the stress level and reducing the hardening slope. The anisotropy also makes the strain extents in the two directions different as was the case in the experiment. The extent of the axial hysteresis is reproduced well while that of the hoop response is longer but still overestimated. Transformation nucleates at the thickness depression on the right between stations (1) and (2) and features weak localized patterns that are normal to the axis of the tube. Unlike the sharp discontinuities in deformation exhibited by biaxiality ratios other than 1.0. here the front is diffuse extending over a length of about 1.5 tube diameters (Fig. 20 of Kazinakis et al. [9]). On unloading, the tube deforms uniformly up to station (7). Subsequently, mild and diffuse localized deformation nucleates on the left without registering on the responses. The front is again orthogonal to the axis of the tube. It is interesting to observe that the deformation profiles in Fig. 2 show also mild inhomogeneity during loading and unloading but with diffuse features oriented along the axis of the tube. A more detailed presentation of the evolution of localization is provided by the video: Video_EquiBiax_Asym+Aniso.mov.

Case II: Isotropic Tension/Compression Asymmetry

We now consider the performance of the analysis in the absence of anisotropy. In this case, the formulation reverts back to that of Jiang et al. [10] with the equivalent strain and strain invariants of Eq. (7) and the other variables listed in the second row of Table 1a. The formulation implies that for the biaxiality ratios other than $\alpha=1$, the calculated results would be influenced by both the partially softening tensile response and the

hardening one in compression in Fig. 4a. Consequently, the predictions exhibit localization that varies with α and stress–strain responses that differ from those measured. The equibiaxial stress state, however, is an exception. Because of isotropy, the diagonal strain tensor is $\mathbf{e}^t = \mathbf{e}_0^t(1,1,-2)^T$. The invariants become: $J_2' = 2\mathbf{e}_0^t$, $J_3' = -2\mathbf{e}_0^t$ and $J_1' = -1$, and therefore $f = f(-1) \equiv 1$, $\xi = 1$ and $\psi^t = \psi_c^t$, and the back stresses take the values in the second row of Table 1b. Or in words, for this stress state the two back stresses and transformation strains coincide and are based exclusively on the uniaxial compressive response.

Adopting this constitutive model in the finite element analysis of the equibiaxial case produces the results in Fig. 6. Fig. 6a plots the responses calculated for the two directions together with the measured ones, and Fig. 6b presents ten deformed configurations with the axial strain superimposed. The two responses are identical exhibiting the monotonic character of the compressive response. The transformation stress is significantly higher, with the stress knee matching the level of the uniaxial compression. However, the predicted hystereses extend to a strain that lies between those measured in the axial and hoop responses. More strikingly, as illustrated by the sequence of deformed configurations, the model tube transforms entirely uniformly throughout the load/unload history.

Case III: Symmetric Model Based on the Compressive Axial Response

The constitutive model is now further specialized to isotropically transforming materials with the same tensile and compressive uniaxial behavior. We first consider a symmetric material with the compressive hardening response in Fig. 4a. In the modeling framework presented, this can be achieved by assigning the weight function ξ in Eq. (6) the value of 1, and setting f=f(-1)=1. This makes the σ^B_{ij} strictly dependent on ψ^t_c as depicted in the third row of Table 1a, and $\varepsilon^t_e=J'_2$. As a result, the model tubes would deform uniformly for all biaxial

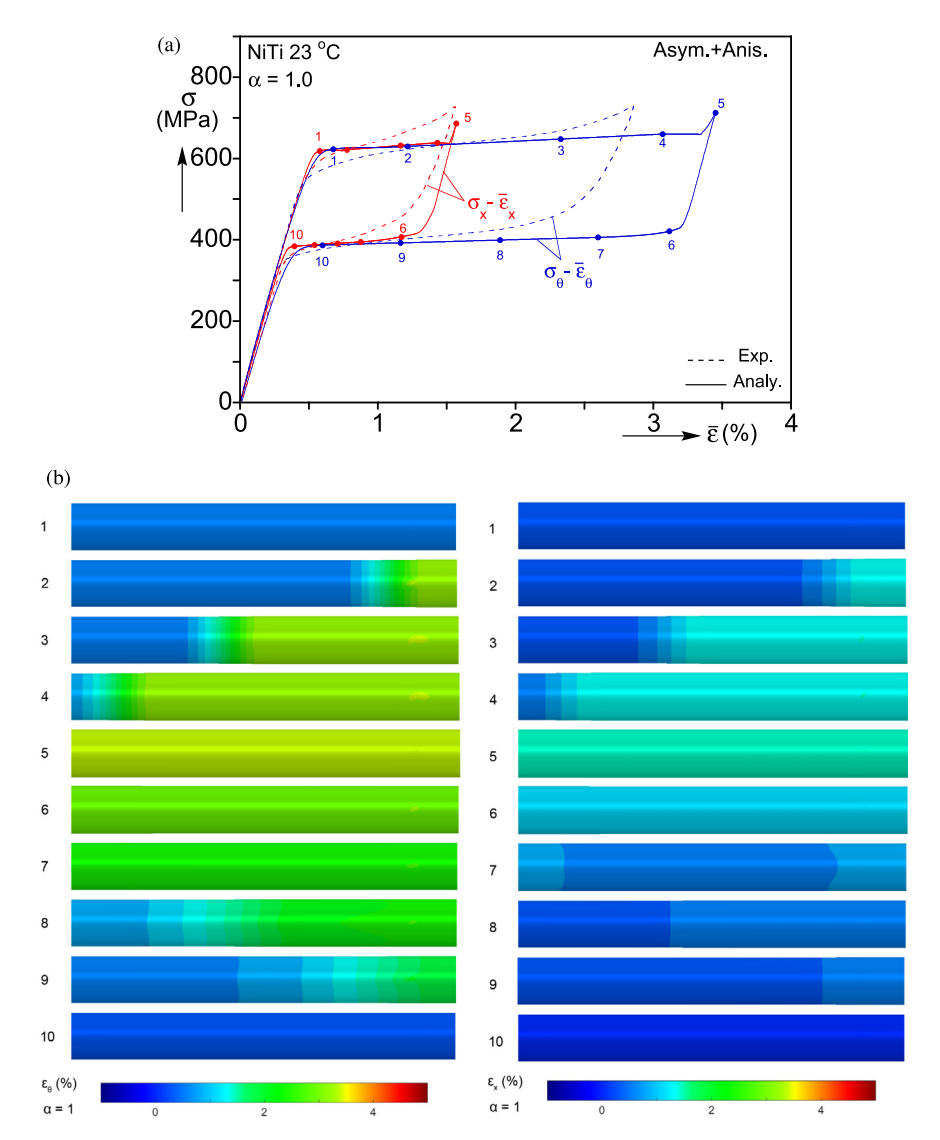


Fig. 5. (a) Stress-average strain responses for equibiaxial loading calculated using the tension/compression asymmetry and anisotropy in the constitutive model, together with the experimental ones. (b) Sequences of calculated axial and hoop strain contours corresponding to the numbered bullets marked on the responses.

loadings, and trace hardening hystereses. For the special case of $\sigma_x = \sigma_\theta$, the main variables take the form listed in the third row of Table 1b, which, not surprisingly, are the same as those of the asymmetric constitutive model specialized to this loading (second row of Table 1b). Hence, for equibiaxial loading the responses and deformation profiles in Fig. 6 hold also for this constitutive model.

Case IV: Symmetric Model Based on the Tensile Axial Response

Conversely, the symmetric constitutive model can be calibrated to the partially softening tensile response in Fig. 4a. This is accomplished by assigning the weight function ξ the value 0, which makes σ_{ij}^B strictly a function of ψ_t^t as shown in the fourth row of Table 1a (note that the equivalent strain becomes $\varepsilon_e^t = J_2'f(1)$). For this model, the dual up-down-up material behavior governs the tube responses for all biaxial loadings considered leading to closed hystereses with stress plateaus and inhomogeneous deformations.

Specializing the constitutive model to the equibiaxial stress state, reduces the main parameters to those in the fourth row of Table 1b. The results of the finite element analysis of a tube loaded under equibiaxial stress are presented in Fig. 7. The calculated stress-average strain responses appear in Fig. 7a and a

set of 16 deformed configurations of the tube with the axial strain superimposed in Fig. 7b. The stresses trace identical closed hystereses with strains extending to nearly 3.5%, which is about one half of the uniaxial transformation strain – a result of the biaxiality. The responses are characterized by stress plateaus during both the forward and reverse transformation. The levels of the two plateaus are significantly lower than those of the measured responses, which in addition exhibited hardening. The most remarkable difference, however, is that for this material model the deformation is strongly inhomogeneous.

Initially, the stresses trace a stiff and stable branch to a local load maximum (station ①). Transformation nucleates as a narrow, nearly circular band of strain of about 3.5% at the site of the small thickness depression on the right. Nucleation leads to sharp drops in the stresses to a plateau of about 465 MPa. As additional volume of fluid is incrementally added to the cavity, the band of higher strain propagates to the right with a nearly circular front orthogonal to the axis of the tube gradually consuming the relatively undeformed section (images ② to just before ③). The small stress oscillations on the plateau are due to the alignment of the planar band with the mesh. The transformation of the last sliver of untransformed material on the left end leads to a

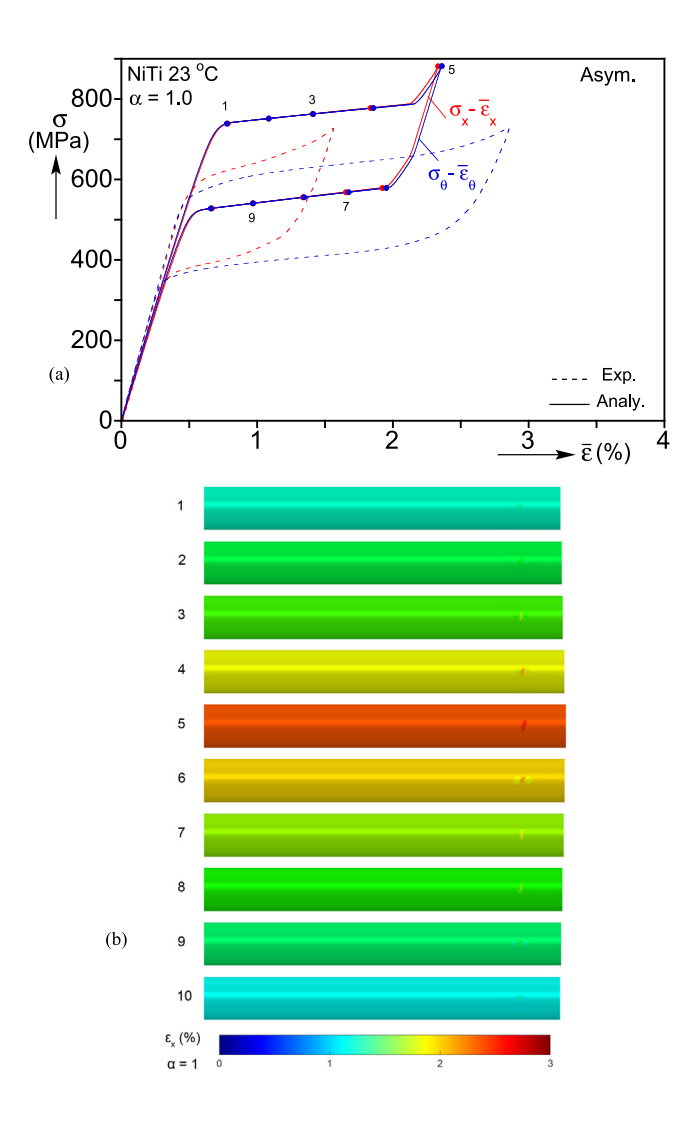


Fig. 6. (a) Stress-average strain responses for equibiaxial loading calculated using the tension/compression asymmetry and isotropy in the constitutive model, and the experimental responses. (b) Sequence of calculated axial strain contours corresponding to the numbered bullets marked on the responses.

small stress valley and subsequently the whole tube is uniformly deformed as it enters the hardening branch of the underlying response in Fig. 4a.

The transformed material unloads homogeneously along a stiff branch down to a stress of 172 MPa when the lower strain phase nucleates at the right boundary of the tube. It quickly morphs into a planar band of about 0.25% strain that is again orthogonal to the axis of the tube. As the volume of fluid inside the cavity is reduced, the relatively sharp front propagates to the right with the stress tracing a plateau of about 235 MPa with similar small oscillations. The last sliver of higher strain material on the left end transforms with a small increase in stress at station (6). A more detailed presentation of the evolution of localization is provided by the video: Video_EquiBiax_SymTens.mov.

4. Concluding remarks

The well-known tension/compression asymmetry exhibited by nearly equiatomic NiTi has been previously modeled using a single surface to describe both the forward and reverse transformation, and by representing uniaxial compression with a hardening

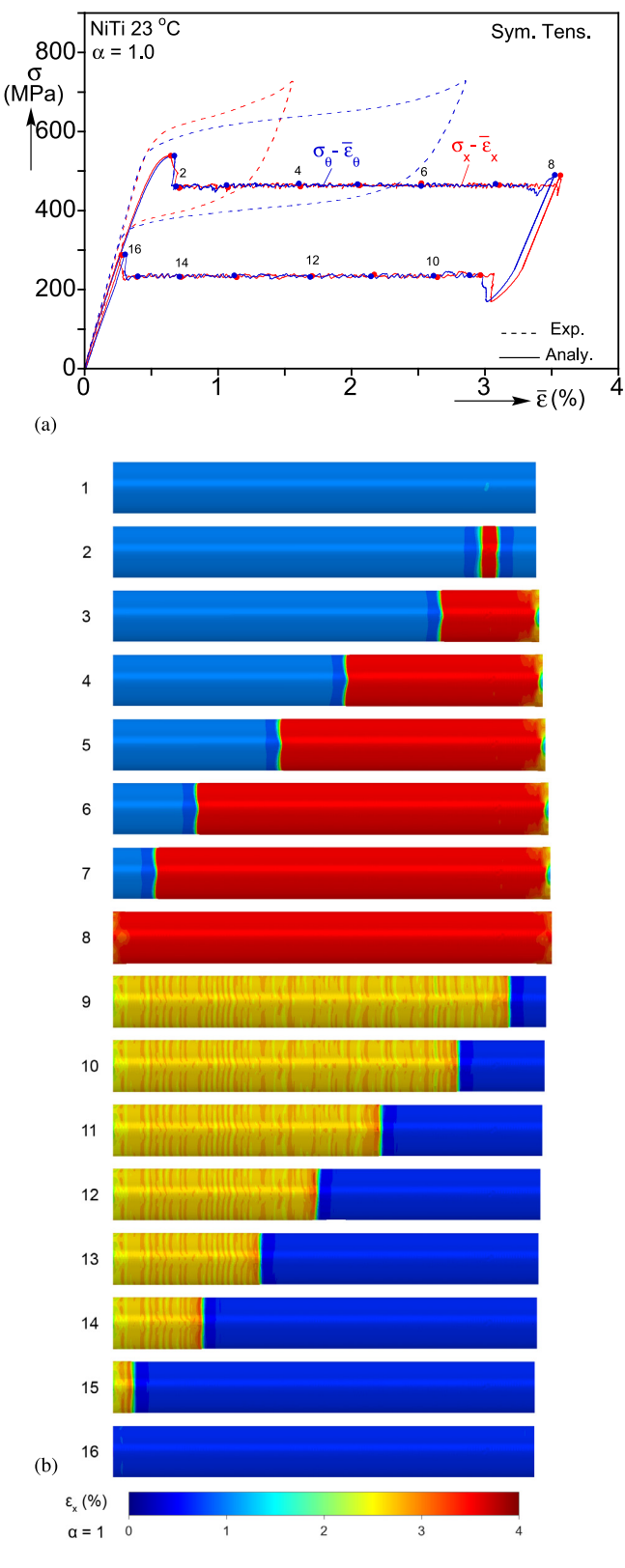


Fig. 7. (a) Stress-average strain responses for equibiaxial loading calculated using the symmetric and isotropic constitutive model calibrated to the axial tensile stress-strain behavior, and the experimental responses. (b) Sequence of calculated axial strain contours corresponding to the numbered bullets marked on the responses.

potential and uniaxial tension with a partially softening one. The two potentials are weighted by a function of the transformation strain. To simulate biaxial stress states. Kazinakis et al. [9] extended the constitutive model to include anisotropy, which was shown necessary for successful simulation of combined internal pressure-axial force experimental results over a range of biaxiality ratios. This letter uses the case of a NiTi tube under equal axial and hoop stress to demonstrate how the tension/compression asymmetry and anisotropy individually and jointly affect its response and the associated localized deformation patterns.

The measured equibiaxial stress-average strain responses exhibit nearly monotonic hystereses and extremely mild homogeneous deformations, but with the hoop transformation strain nearly double that in the axial direction. For this stress state, when the asymmetric constitutive model is isotropic, the influence of the uniaxial tensile behavior is removed, and the calculated responses are strictly governed by the compressive one. The hoop and axial hystereses coincide, exhibit much higher transformation stresses, more pronounced hardening, and transformation strains that lie between those measured. When anisotropy is added to the model, the analysis produces monotonic hystereses with transformation stresses down to the level of the measured ones, matches the strain extent of the axial response. and overpredicts the hoop strain to some extent. The hardening is somewhat lower than that of the experiment, which allows a weak, diffuse front of localized deformation to develop.

In the absence of the tension/compression asymmetry and anisotropy in the constitutive model, the calculated responses depend on the uniaxial material response to which the model calibrated. When calibrated to the stable compressive stressstrain response, the analysis produces hardening responses and homogeneous deformation for all biaxial stress states. For the equibiaxial stress, the results are identical to those of the isotropic asymmetric model. By contrast, when calibrated to the partially unstable tensile stress-strain response, the analysis generates stress plateaus with inhomogeneous deformation of helical bands for all biaxial stress states. For the equibiaxial stress state, the axial and hoop stress-average strain responses are again the same, and transformation leads to the coexistence of two deformation regimes separated by a front that is orthogonal to the axis of the tube.

The study demonstrates that the behavior of NiTi under biaxial stress states requires proper modeling of the tension/compression asymmetry as well as any inherent anisotropy.

Declaration of competing interest

The authors declare that they have no known competing financial interests or personal relationships that could have appeared to influence the work reported in this paper.

Acknowledgments

The authors acknowledge with thanks the financial support received for this work from the National Science Foundation, United States under grant no. CMMI-1762389. The literature on the modeling of shape memory alloys is extensive, so in this letter only works directly impacting the subject at hand are cited.

Appendix A. Constitutive model calibration

The back stress potentials ψ_t^t and ψ_t^t are respectively calibrated for best fitting of the compressive and tensile stress-

average strain responses using the following expression:
$$\frac{d\psi_{ct}^t}{d\tilde{\varepsilon}_e^t} = h_0 \tilde{\varepsilon}_e^t + (h_1 - h_0) \left[\tilde{\varepsilon}_e^t - \frac{1}{b} (1 - e^{-b\tilde{\varepsilon}_e^t}) \right]$$

$$+ (h_2 - h_1)(\varepsilon_2 - \varepsilon_1)$$

$$= \begin{cases} 0 & \tilde{\varepsilon}_e^t \leq \varepsilon_1 \\ (2.5\zeta^4 - 3\zeta^5 + \zeta^6) & \varepsilon_1 \leq \tilde{\varepsilon}_e^t \leq \varepsilon_2 \\ 0.5 + \zeta & \varepsilon_2 \leq \tilde{\varepsilon}_e^t \end{cases}$$
 (A.1)

where $\zeta = (\tilde{\varepsilon}_e^t - \varepsilon_2)/(\varepsilon_2 - \varepsilon_1)$ and $\{b, h_0, h_1, h_2, \varepsilon_1, \varepsilon_2\}$ are fitting parameters listed in Table A.1.

Table A.1 Model parameters for axial tensile and compressive responses.

Model	E GPa	ν	σ_o MPa	b	h ₀ GPa	h ₁ GPa	h ₂ GPa	ε ₁ %	ε ₂ %
	66.3 66.3					-11.4 2.78		3.0 3.0	3.4 3.4

Appendix B. Supplementary data

Supplementary material related to this article can be found online at https://doi.org/10.1016/j.eml.2022.101689.

References

- [1] N.J. Bechle, S. Kyriakides, Localization in NiTi tubes under bending, Int. J. Solids Struct. 51 (2014) 967-980, http://dx.doi.org/10.1016/j.ijsolstr.2013.
- [2] K. Jacobus, H. Sehitoglu, M. Balzer, Effect of stress state on the stress-induced martensitic transformation of polycrystalline Ni-Ti Alloy, Metall. Mater. Trans. A 27 (1996) 3066-3073, http://dx.doi.org/10.1007/ BF02663855
- [3] L. Orgéas, D. Favier, Stress-induced martensitic transformation of a NiTi alloy in isothermal shear, tension and compression, Acta Mater. 46 (1998) 5579-5591, http://dx.doi.org/10.1016/S1359-6454(98)00167-0.
- [4] B. Reedlunn, C.B. Churchill, E.E. Nelson, J.A. Shaw, S.H. Daly, Tension, compression, and bending of superelastic shape memory tubes, J. Mech. Phys. Solids 63 (2014) 506-537, http://dx.doi.org/10.1016/j.jmps.2012.12.
- [5] N.J. Bechle, S. Kyriakides, Evolution of localization in pseudoelastic NiTi tubes under biaxial stress states, Int. J. Plast. 82 (2016) 1-31, http://dx. doi.org/10.1016/j.ijplas.2016.01.017.
- D. Helm, P. Haupt, Thermomechanical behavior of shape memory alloys, in: Proc. SPIE Int'l Symp. Smart Struct. Mat., Vol. 8, 2001, pp. 302-313, http://dx.doi.org/10.1117/12.432769.
- [7] O.P. Sun, Z.Q. Li, Phase transformation in superelastic NiTi polycrystalline micro-tubes under tension and torsion—from localization to homogeneous deformation, Int. J. Solids Struct. 39 (2002) 3797-3809, http://dx.doi.org/ 10.1016/S0020-7683(02)00182-8.
- B. Reedlunn, W.S. LePage, S.H. Daly, J.A. Shaw, Axial-torsion behavior of superelastic tubes: Part I, proportional isothermal experiments, Int. J. Solids Struct. 199 (2020) 1-35, http://dx.doi.org/10.1016/j.ijsolstr.2020.03.018.
- K. Kazinakis, Kyriakides, C.M. Landis, Simulation of the response and evolution of localization in pseudoelastic NiTi tubes under biaxial stress states, Int. J. Plast. 151 (2022) 103179, http://dx.doi.org/10.1016/j.ijplas. 2021.103179.
- [10] D. Jiang, N. Bechle, C.M. Landis, S. Kyriakides, Buckling and recovery of NiTi tubes under axial compression, Int. J. Solids Struct. 80 (2016) 52-63, http://dx.doi.org/10.1016/j.ijsolstr.2016.07.003.
- [11] D. Jiang, C.M. Landis, S. Kyriakides, Effects of tension/compression asymmetry on the buckling and recovery of NiTi tubes under axial compression. Int. J. Solids Struct. 100-101 (2016) 41-53, http://dx.doi.org/10.1016/j.ijsolstr. 2016.07.003.
- [12] D. Jiang, S. Kyriakides, N.J. Bechle, C.M. Landis, Bending of pseudoelastic NiTi tubes, Int. J. Solids Struct. 124 (2017) 192-214, http://dx.doi.org/10. 1016/j.ijsolstr.2017.06.032.
- [13] D. Jiang, C.M. Landis, A constitutive model for isothermal pseudoelasticity coupled with plasticity, in: Shape Memory and Superelasticity, Vol. 2, 2016, pp. 360-370, http://dx.doi.org/10.1007/s40830-016-0078-8.
- [14] J.F. Hallai, S. Kyriakides, Underlying material response for Lüders-like instabilities, Int. J. Plast. 47 (2013) 1-12, http://dx.doi.org/10.1016/j.ijplas. 2012.12.002.